

NUMERICAL ANALYSIS OF THE BOILING HEAT TRANSFER COEFFICIENT IN THE FLOW IN MINI-CHANNELS

Beata MACIEJEWSKA*, Sylwia HOŻEJOWSKA*, Mirosław GRABOWSKI**, Mieczysław E. PONIEWSKI**

*Faculty of Management and Computer Modelling, Department of Mathematics and Physics,
Kielce University of Technology, Al.1000-lecia P.P. 7, 25-314 Kielce, Poland

**Institute of Mechanical Engineering, Warsaw University of Technology,
Plock Campus, ul. Łukasiewicza 17, 09-400 Plock, Poland

beatam@tu.kielce.pl, ztpsf@tu.kielce.pl, Miroslaw.Grabowski@pw.edu.pl, Mieczyslaw.Poniewski@pw.edu.pl

received 28 February 2023, revised 31 May 2023, accepted 16 June 2023

Abstract: This paper deals with boiling heat transfer in the flow of water through an asymmetrically heated horizontal rectangular mini-channel. The mini-channel was made by gluing three transparent glass plates and a copper block. Through the glass window, the variable along the length of the mini-channel two-phase flow structures were recorded to determine local values of the void fraction. Four resistance heaters were attached to the copper block, powered by direct current, generating the heat initiating the flow boiling inside the channel. During the experiment, the following were measured: water volumetric flow rate, inlet pressure with pressure drop, inlet and outlet water temperature, copper block temperatures at three points inside its body, voltage and current supplied to the heaters. Stationary and laminar fluid flow with low Reynolds numbers were assumed in the mathematical model of heat transfer in selected elements of the measuring module. The temperature distributions in the copper block and flowing water were described by the appropriate energy equations: the Laplace equation for the copper block and the Fourier–Kirchhoff equation with parabolic fluid velocity for the flowing water. These equations were supplemented with a set of boundary conditions based on measurement data; moreover, data from experimental studies were the basis for numerical calculations and their verification. Two-dimensional temperature distributions of the copper block and water were calculated with the Trefftz method (TM). The main objective of this study was to determine the heat transfer coefficient on the contact surface of the copper block and water, which was calculated from the Robin boundary condition. The results of the calculations were compared with the results of numerical simulations performed using the Simcenter STAR-CCM+ software, obtaining consistent values. Computational fluid dynamics (CFD) simulations were verified based on experimental data including void fraction and temperature measurements of the copper block and flowing water.

Key words: flow boiling, void fraction, heat transfer coefficient, Simcenter STAR-CCM+, CFD, Trefftz method

1. INTRODUCTION. BRIEF STATE OF THE ART

Boiling heat transfer in mini-channel flow has been the subject of extensive experimental and numerical research presented in the literature [1–11]. Due to the complexity of the process, the development of comprehensive correlations and/or flow boiling models based solely on experimental data is not possible. The use of numerical simulation in the modelling thermal and flow phenomena allows estimating the approximate values of physical parameters (e.g. temperature or pressure) and examining their impact on the studied phenomenon [8–11]. Numerical simulation also reduces the time needed for time-consuming and costly experimental investigation. However, it should be noted that the results of numerical simulations should always be verified based on the results of the experiment.

Experimental studies of flows in mini- and micro-channels focus on boiling flow and, to a lesser extent, condensation. Flow modelling with change of fluid phase is hampered by the fact that these flows are described on a macroscopic scale as stationary, but the formation, growth, coagulation and collapse of vapour bubbles generate local non-stationary changes in temperature,

pressure and flow velocity. Complex two-phase boiling flow models require numerous simplifying assumptions or hard-to-measure experimental data. For this reason, numerous models of specific boiling flow cases have been developed, such as the three-zone model for the case of flow of elongated bubbles [12,13] or the model for annular flow [9], both of which are the characteristic flows for mini- and micro-channels. The Lagrangian–Eulerian framework with finite element method (FEM) requires a laborious and complicated numerical procedure for a one-fluid model and thus has limited applicability [14].

The briefly described state of modelling and numerical simulation indicates the necessity for invention of a general and specific model of flow boiling in mini-channels as well as corresponding computation methods. The most common methods used in flow boiling in mini-channels include correlation equations, the Galerkin FEM, volume of fluid (VOF) method, lattice Boltzmann methods (LBM), the Trefftz method (TM) and the recently rapidly developing computational fluid dynamics (CFD) methods. The description of the current experimental and numerical approaches to the analysis of heat transfer in mini- and micro-channels can be found in the literature [5,15–18]. A particularly important parameter for the description of flow boiling is the local value of the void fraction, which causes the search for various non-intrusive methods of its measurement. In these methods, it is important that the measur-

ing transducer does not disturb the flow and does not affect the observed two-phase structure. Methods that meet this condition are usually based on the use of changes in certain physical parameters of the flowing fluid related to the void fraction, e.g. change in the dielectric constant of the two-phase mixture (capacitance method [19–21]), change in the acoustic properties of the two-phase mixture for ultrasonic wave propagation [22] and optical methods based on image analysis, which are often used in experimental studies of two-phase flows in mini-channels [18]. An extended overview of experimental techniques and correlations for the void fraction can be found in the literature [23].

In the presented experimental research, the new approach concerning high-speed filming with a high-resolution camera, specific photographic data reduction and experimental errors analysis of the observed two-phase boiling flow structures in a horizontal, rectangular mini-channel [3] was applied. This technique allowed simultaneous boiling two-phase flow visualisation and local void fraction measurement.

In the paper, the results were obtained using the TM and numerical simulation performed in the CFD environment. The choice of methods results from the main goal of the article, which is to formulate and solve a mathematical model concerning the heat transfer problem in flow boiling in mini-channels.

The TM, compared to traditional numerical methods, offers advantages in terms of computational efficiency and accuracy. By utilising Trefftz functions, which are solutions to the governing equations, the method can provide highly accurate results, with fewer computational resources. The TM is a meshless method that allows for stable solutions to inverse heat transfer problems and does not require advanced software. Numerical simulations performed using CFD codes enable predictions and analysis of temperature distributions of heaters elements and working fluid in exchanges. This allows to gain deeper insights into the physics of the system and identify any heat transfer inefficiencies.

In the paper, the results of numerical simulations were compared with the results of the TM. Overall, the Trefftz and Simcenter STAR-CCM+ results are coincident. In the future, the TM can be used to validate, together with experimental data, the results of numerical simulations carried out on commercial CFD codes.

2. EXPERIMENTAL APPARATUS AND PROCEDURE

2.1. Experimental apparatus

The diagram of the experimental apparatus is shown in Fig. 1. The mini-channel, which is the basic element of the apparatus, was created by gluing three transparent glass plates and a rectangular milled copper block, as shown in Fig. 1b. The copper block forms the structural basis for the mini-channel and acts as a thermal buffer, ensuring equalisation of the temperature field. One of the surfaces of the block is the heating surface in the mini-channel (Fig. 1b). Heat is generated by four flat heating resistors placed on the outer surface of the copper block opposite the heating surface in the mini-channel.

The heating resistors were powered by a TDK Lambda GEN 50–30 high-current DC power supply. Optiwhite glass was chosen as the construction material for the walls of the mini-channels. It is colourless, contains a limited amount of iron and has a high light transmission factor. To illuminate the channel, a proprietary illumina-

tor system based on Citizen CL-L233-HC13L1-C LED elements was used. LOCTITE® SI 5145 adhesive was used to glue the mini-channel glass and copper elements. The dimensions of the mini-channel are as follows: length 180 mm, width 4 mm and depth 1.5 mm, with a cross-section of 6 mm². The hydraulic diameter of the mini-channel is 2.18 mm, as shown in Fig.1b. Five thermocouples were placed in the mini-channel module, one at the inlet, one at the outlet of the mini-channel and three inside the copper heating block (Fig. 1b). Two pressure sensors were placed at the inlet and outlet of the channel. The flow of distilled water was generated by a precision gear pump and reached a maximum values of 1.5×10^{-7} m³/s. The flow in the mini-channel was laminar, where $Re = 198$. Flows at low Reynolds numbers are quite often used in miniature cooling systems for electronic devices.

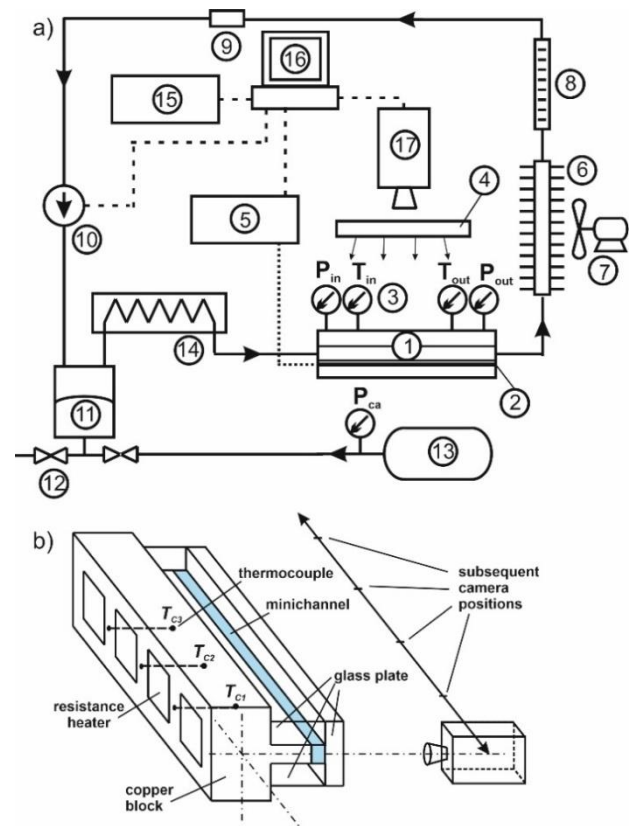


Fig. 1. (a) Scheme of the experimental apparatus: 1 – measurement module with a mini-channel, 2 – copper heating block, 3 – temperature and pressure sensors [Czaki K-type, TP-201; Kobold, 0–2.5 bar], 4 – LED lighting, 5 – DC power supply [TDK Lambda], 6 – cooler, 7 – fan, 8 – rotameter [Heinrichs], 9 – filter, 10 – precision gear pump [Tuthill Concord DGS 38 PP], 11 – pressure control, 12 – compressed air valves, 13 – compressed air tank, 14 – preheater, 15 – control and measurement module [NI cDAQ-9178 chassis], 16 – computer controlling the experiment with a LabView script, 17 – high-speed video camera [Phantom 711, Vision Research], P_{ca} – compressed air pressure sensor; T_{in}, P_{in} temperature, pressure at the inlet to the channel, T_{out}, P_{out} temperature, pressure at the outlet of the channel, (b) General view of the mini-channel: TC1, TC2 i TC3 thermocouples located inside the copper heating block

Figs. 2 and 3 show the view of the test stand and the measurement module with a mini-channel, respectively.

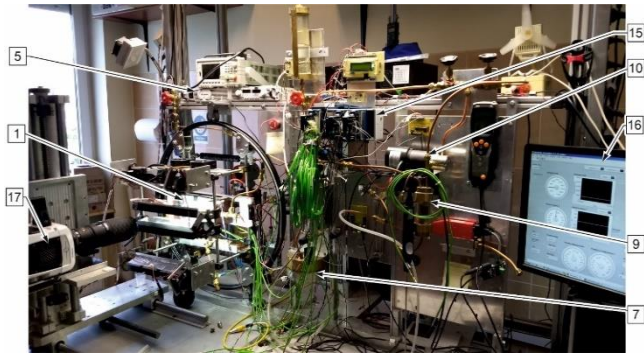


Fig. 2. View of the experimental setup, markings as in Fig. 1



Fig. 3. View of the measuring module with mini-channels, markings: 1a – mini-channel, 18 – radiator of the LED illuminator, other markings as in Fig. 1.

2.2. Experimental procedure

The measurement procedure used for the experiments performed at the stand (Fig. 1) is as follows:

- (a) Pumping the fluid through the mini-channel at the set volumetric flow rate, inlet temperature and pressure.
- (b) Two-stage heating of the fluid up to the boiling point by using a preheater, followed by a heating copper block for the mini-channel.
- (c) Recording of the basic thermal and flow parameters: water volumetric flow rate, water inlet and outlet temperatures, inlet pressure, pressure drop along the length of the mini-channel, power supply to the heater and temperature in three points of the copper heater. A single measurement had the following course: within 6–7 s, all experimental parameters were read and saved to a computer disk.
- (d) Filming two-phase flow structures with a high-speed video camera and saving the recorded file to a computer disk.

Images of two-phase flow structures recorded by a high-speed camera were used to determine the local void fraction in the channel, as mentioned in papers [3,7]. This was achieved by a specially developed procedure based on image analysis on the MatLab environment.

3. MATHEMATICAL MODEL AND CALCULATION METHODS

This paper study proposes two approaches to determine the heat transfer coefficient between a copper heating surface and distilled water flowing in a mini-channel. In the first approach, it was assumed that the temperature distribution of the copper block

satisfies the Laplace equation, and the water temperature satisfies the corresponding the energy equation with one component of the velocity vector (with other components equal to zero) parallel to the direction of fluid flow. The given energy equations have been supplemented with an appropriate set of resulting boundary conditions from measurement data. The semi-analytical TM [24] was used to determine the two-dimensional temperature distributions of the copper block and water. The idea behind the TM is to approximate the unknown solution of a partial differential equation with a linear combination of functions (these are the Trefftz functions) that satisfy the equation exactly. Knowing the boundary conditions allows determining the coefficients of a linear combination based on the least squares method. The approximation obtained in this way is a continuous and differentiable function that satisfies the governing equation in an exact manner and the boundary conditions in an approximate manner. In the presented approach, the knowledge of the temperature distribution of the copper block and water allows determining the heat transfer coefficient at the copper block surface–water interface from the Robin boundary condition. A wide range of applications of the TM for solving direct and inverse engineering problems can be found in articles and monographs, e.g. [25–30].

In the second approach, as in [31], Simcenter STAR-CCM+ software was used to analyse the heat transfer in the measurement module. The geometrical dimensions of the heating copper block and the physical parameters of both the material of the block and the flowing fluid were used in the numerical calculations, as well as the spatial orientation of the entire measurement module and the thermal and flow parameters recorded during the experiment.

It is important to note that the TM and CFD simulations have advantages and limitations, and the choice between the two methods depends on the specific problem at hand, the available resources and the desired accuracy and scope of the solution. Tab. 1 shows the differences between the Simcenter STAR-CCM+ simulation and the TM.

Tab. 1. Differences between the Simcenter STAR-CCM+ simulation and the TM

Differences	CFD simulation	TM
Need meshing	+	-
Solution satisfies the governing equation	Approximately	Exactly
Used to solve non-linear equations	+	– *)
Domain	No limitations on shape	Simple shape **)
Computer	Requires large processing power	Does not require large processing power and advanced software

*)Combination of the TM with other methods (e.g. FEM, Picard method) enables solving non-linear equations.

**)Geometrically complex domain can be divided into simple subdomains.

3.1. Trefftz method

The model given below is a simplified version of the model described in [7], where it was assumed that the measurement mod-

ule is in a steady state and the heat transfer process in the copper block and water is carried out in two directions: x (referring to the length of the block and the mini-channel) and perpendicular to it, y (referring to the height of the block and the depth of the mini-channel δ_M). As in [7], assuming that the physical phenomena occurring on the side edges of the module do not significantly affect the thermodynamics of the process taking place in the central part of the module, further considerations concerned only the central part of the measurement module, i.e. the section along its length. A laminar flow with one velocity component $v(y)$ with a parabolic profile fulfilling the condition was assumed in the channel:

$$\frac{1}{\delta_M} \int_0^{\delta_M} v(y) dy = v_{ave} \quad (1)$$

where δ_M is the mini-channel depth, $v(y)$ is the parabolic water velocity and v_{ave} is the average speed of water in the mini-channel based on the known volume flow.

The model assumes that the temperature of the copper block and water satisfies the Laplace equation and the Fourier–Kirchhoff equation, respectively, in the appropriate forms:

- For a copper block in the domain,

$$D_c = \{(x, y) \in R^2 : 0 < x < L, 0 < y < \delta_c\}$$

$$\nabla^2 T_c = 0 \quad (2)$$

- For water in the domain,

$$D_f = \{(x, y) \in R^2 : 0 < x < L, \delta_c < y < \delta_c + \delta_M\}$$

$$\lambda_f \nabla^2 T_f = v(y) c_p \rho_f \frac{\partial T_f}{\partial x} \quad (3)$$

where T_c is the copper block temperature, δ_c is the copper block depth, L is the length of the measurement module, T_f is liquid (water temperature), λ_f is the water thermal conductivity, ρ_f is the water density and c_p is the water specific heat. For Eqs (2) and (3), the appropriate Dirichlet and Neumann boundary conditions were adopted. Following boundary conditions were assumed for Eq. (2):

- the temperature of the block T_{Ck} is known from the measurements in its three inner points (x_k, δ_{mp}) (Fig. 1b)

$$T_c(x_k, \delta_{mp}) = T_{Ck} \text{ for } k = 1, 2 \quad (4)$$

- its outer wall and walls perpendicular to the mini-channel are insulated

$$\frac{\partial T_c(x, 0)}{\partial y} = 0 \quad (5)$$

$$\frac{\partial T_c(0, y)}{\partial x} = 0 \quad (6)$$

$$\frac{\partial T_c(L, y)}{\partial x} = 0 \quad (7)$$

- heat exchange takes place on the contact surface with the resistors, i.e. for $x \in D$, where $D = \langle 2.5 \text{ mm}; 41.5 \text{ mm} \rangle \cup \langle 47.5 \text{ mm}; 86.5 \text{ mm} \rangle \cup \langle 93.5 \text{ mm}; 132.5 \text{ mm} \rangle \cup \langle 139.5 \text{ mm}; 178.5 \text{ mm} \rangle$

$$\lambda_c \frac{\partial T_c(x, 0)}{\partial y} = -q \quad (8)$$

where q is the heat flux and λ_c is the copper thermal conductivity.

The following assumptions constitute a set of boundary conditions for Eq. (3):

- ideal thermal contact between the copper block and the water

$$T_c(x, \delta_c) = T_f(x, \delta_c) \quad (9)$$

$$\lambda_c \frac{\partial T_c(x, \delta_c)}{\partial y} = \lambda_f \frac{\partial T_f(x, \delta_c)}{\partial y} \quad (10)$$

- the knowledge of water temperature at the entrance and exit to/from the mini-channel

$$T_f(0, y) = T_{f,in} \quad (11)$$

$$T_f(L, y) = T_{f,out} \quad (12)$$

where $T_{f,in}$ is the water temperature at the inlet to the mini-channel and $T_{f,out}$ is the water temperature at the outlet from the mini-channel.

The system of differential equations defined in this way together with the boundary conditions leads to the solution of two inverse Cauchy-type problems [25,32] in two different regions (copper block and mini-channel) with different shapes and physical parameters. To determine the two-dimensional temperature distributions of the copper block and water, the TM described in detail in [28,29] was used. The knowledge of temperature distribution in both areas allows determining the heat transfer coefficient of on their contact surface from the Robin boundary condition:

$$\alpha(x) = \frac{-\lambda_c \frac{\partial T_c}{\partial y}(1-\varphi(x))}{T_c - T_{f,ave}} \quad (13)$$

where $T_{f,ave}$ is the reference water temperature and φ is the local void fraction.

Reference water temperature $T_{f,ave}$ was calculated as the average water temperature in the mini-channel, and the local void fraction φ was approximated by the logistic curve in further calculations.

3.2. Simcenter STAR-CCM+ software

To verify the calculation results obtained by using the TM, the temperature distribution of the copper block and water and the value of the heat transfer coefficient were calculated using Simcenter STAR-CCM+ software (version 2020.2.1 (15.04.010-R8)).

The calculations assume that (i) the fluid flow is incompressible with a known constant flow rate, (ii) the temperature of the fluid at the inlet to the mini-channel and its overpressure at the outlet are known, (iii) the temperature of the copper block at three measurement points is known (Fig. 1b), (iv) there is no heat losses to the surroundings, (v) the heat flux delivered to the resistors is known and (vi) the material properties do not depend on temperature.

A PC with an Intel Core i9 CPU (24 cores), clocked at 3.50 GHz and 256 GB of RAM, was used for the calculations. The polyhedral computational grid in the entire module was created from 7,573,690 cells (the grid in the mini-channel consisted of 340,198 cells), as shown in Fig. 4. The material parameters used in the calculations are presented in Tab. 2.

Numerical calculations were performed using the multiphase VOF model found in the literature [33]. In this approach, the issues of heat transfer and fluid flow are described by the equations of mass, momentum and energy balances and the void fraction in a two-phase mixture. The problem formulated in this way is solved by the finite volume method (FVM) [34], which consists in discretising the integral form of given equations to a system of algebraic equations. Values of functions in nodes located in the centres of

control areas equivalent to the cells of the calculation grid are sought.

Tab. 2. Material parameters of the measurement module

Element of the measuring module			
Material parameter	Cooper block	Heater	Distilled water
Density [kg/m ³]	8,940.0	7,832.0	997.561
Dynamic viscosity [Pa/s]	-	-	0.00088871
Specific heat [J/kg/K]	386.0	434.0	4,181.72
Thermal conductivity [W/m/K]	398.0	63.9	0.620271

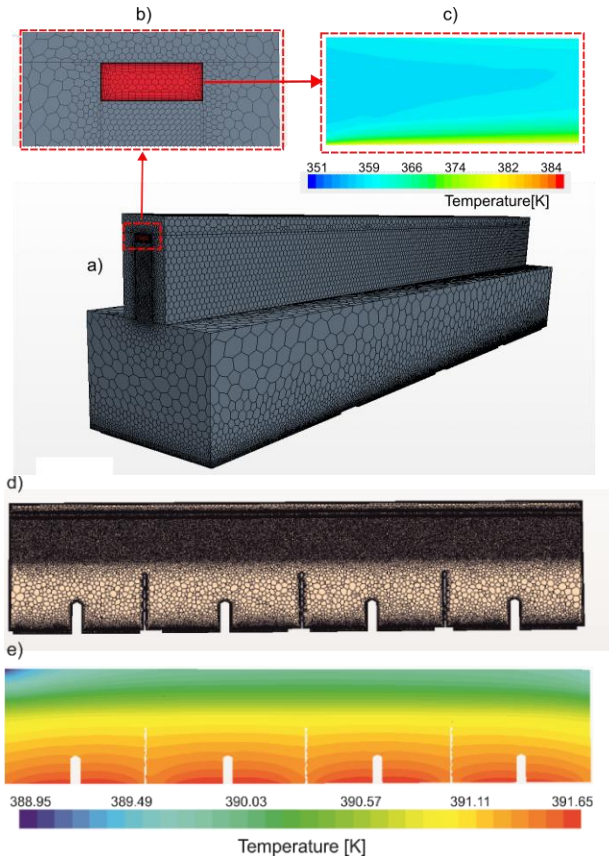


Fig.4. (a) Calculation grid applied to the mini-channel with the heating block, (b) enlargement of the cross-section at the entrance to the mini-channel, (c) water temperature at a distance of 0.0045 m from the inlet to the mini-channel, (d) middle cross-section of the mini-channel with the heating block along their length, (e) heating block temperature in the middle cross-section

Systematic refining of the grid size is important for computer simulations.

The grid convergence method (GCI) [35,36], based on the Richardson extrapolation (RE) [37,38], was used to examine and evaluate the quality of the adopted computational grid. According to the procedure for estimation of discretisation error described in the literature [36] and recommended by the Fluids Engineering Division of the American Society of Mechanical Engineers (ASME), the grid convergence index for the 3D grid has the following form:

$$GCI_{ij} = \frac{1.25e_{ij}}{r_{ij}^{p-1}} \quad (14)$$

where

$$e_{ij} = \left| \frac{\phi_i - \phi_j}{\phi_i} \right| \quad (15)$$

while ϕ_k denotes the solution on the k th grid.

The grid refinement factor r in Eq. (14) was calculated according to the following formula:

$$r_{ij} = \frac{h_i}{h_j} \text{ for } h_j < h_i \quad (16)$$

while the order p of the method is the solution of the following equation:

$$p - \frac{\ln \left(\frac{\epsilon_{32}}{\epsilon_{21}} \right) + \ln \left(\frac{r_{21}^{p-1} - \text{sgn} \left(\frac{\epsilon_{32}}{\epsilon_{21}} \right)}{r_{32}^{p-1} - \text{sgn} \left(\frac{\epsilon_{32}}{\epsilon_{21}} \right)} \right)}{\ln(r_{21})} = 0 \quad (17)$$

where representative grid size h for the 3D grid was calculated from the following formula:

$$h = \left[\frac{1}{N} \sum_{i=1}^N (\Delta V_i) \right]^{1/3} \quad (18)$$

and V_i is the volume of the i th cell and N is the total number of cells used for the computations, while

$$\epsilon_{ij} = \phi_i - \phi_j \quad (19)$$

where ϕ_k is defined as in Eq. (15).

Calculations should be carried out for at least three different grids such that the grid refinement factor r should be >1.3 [36]. Additional extrapolated values can be taken from:

$$\phi_{ij}^{ext} = \frac{r_{ij}^p \phi_j - \phi_i}{r_{ij}^p - 1} \quad (20)$$

and

$$e_{ij}^{ext} = \left| \frac{\phi_{ij}^{ext} - \phi_j}{\phi_{ij}^{ext}} \right| \quad (21)$$

The aim of the calculation was the numerical uncertainty $GCI_{2,1}$ in the fine-grid solution, which is the basis for generating the results presented in the article. Tab. 3 illustrates results of this calculation procedure for three selected grids.

Tab. 3. Values of parameters in calculations of discretisation error

Parameter	Experiment 1 $q = 7.80 \text{ kW/m}^2$	Experiment 2 $q = 21.90 \text{ kW/m}^2$	Experiment 3 $q = 26.52 \text{ kW/m}^2$
N_1	7,573,690	7,573,690	7,573,690
N_2	2,837,607	2,837,607	2,837,607
N_3	1,251,945	1,251,945	1,251,945
r_{21}	1.39	1.39	1.39
r_{32}	1.31	1.31	1.31
ϕ_1	381.59 K	390.42 K	382.43 K
ϕ_2	381.69 K	390.77 K	382.30 K
ϕ_3	381.83 K	391.30 K	382.26 K
p	1.4	2	2.9
ϕ_{21}^{ext}	381.40 K	390.04 K	382.51 K
e_{21}	0.10%	0.30%	0.12%
e_{32}	0.12%	0.44%	0.03%
e_{21}^{ext}	0.17%	0.32%	0.07%
$GCI_{2,1}$	0.21%	0.40%	0.09%

Eq. (14) is interpreted as an uncertainty estimate of discretisation error [39], whereas Eqs (15) and (21) express the value of the approximate relative error. For the calculation of a more conservative estimate uncertainty of the discretisation error, authors of Report INL/EXT-06-11789 TRN: US0800104 [40] suggest the following formula:

$$\delta = \frac{1}{4}(e_{21} + e_{32} + e_{21}^{ext} + GCI_{21}) \quad (22)$$

The confidence interval (at a confidence level $(1 - \alpha) * 100\%$, here $\alpha = 0.05$) of the estimate of the discretisation error was defined as follows:

$$(\max(0, \delta - s t_{\alpha/2}), \delta + s t_{\alpha/2}) \quad (23)$$

where s is the estimate of the standard deviation of all the values calculated from Eqs (14), (15) and (21), and $t_{\alpha/2}$ is calculated from T-distribution. For $\alpha = 0.05$ (confidence level is equal to 95%) and the T-distribution with 3 degrees of freedom, the value of the coverage factor $t_{\alpha/2}$ is equal to 3.182.

Values of parameters lead to obtain the confidence interval defined by Eq. (23), as given in Tab. 4.

Tab. 4. Values of parameters in calculations of the estimate of the numerical uncertainty

Parameter	Experiment 1 $q = 7.80 \text{ kW/m}^2$	Experiment 2 $q = 21.90 \text{ kW/m}^2$	Experiment 3 $q = 26.52 \text{ kW/m}^2$
δ	0.0015	0.0037	0.0008
s	0.0005	0.0007	0.0003
$s t_{\alpha/2}$	0.0016	0.0022	0.0011

As can be seen from Tab. 4, expanded uncertainty (at the confidence level of 95%) of the discretisation error for the three selected grids in presented experiments varies from 0.19% to 0.59%.

4. RESULTS

The values of other experimental parameters used in the calculations along with their measurement errors are presented in Tabs. 2 and 5.

Tab. 5. Values of experimental parameters and their measurement errors

Parameter	Variation range of the parameter	Experimental error
Inlet pressure [kPa]	5.33–26.33	1.25
Pressure drop [Pa]	20.25–108.17	3.75
Inlet temperature [K]	352–362	0.5
Outlet temperature [K]	374–382	0.5
Average inlet subcooling [K]	17.10	0.5
Copper block temperature at the measuring points [K]	$T_{C1}: 382.03\text{--}391.10$ $T_{C2}: 382.92\text{--}391.96$ $T_{C3}: 382.89\text{--}391.45$	0.5
Ambient temperature [K]	294	0.5

Heat flux [kW/m^2]	7.80–26.52	6%
Mass flux [$\text{kg/m}^2\text{s}$]	11–111.9	7.8%

Fig. 5 lists the values of the experimentally determined void fraction, its approximation with the logistic curve and the results obtained from the simulations performed in STAR-CCM+.

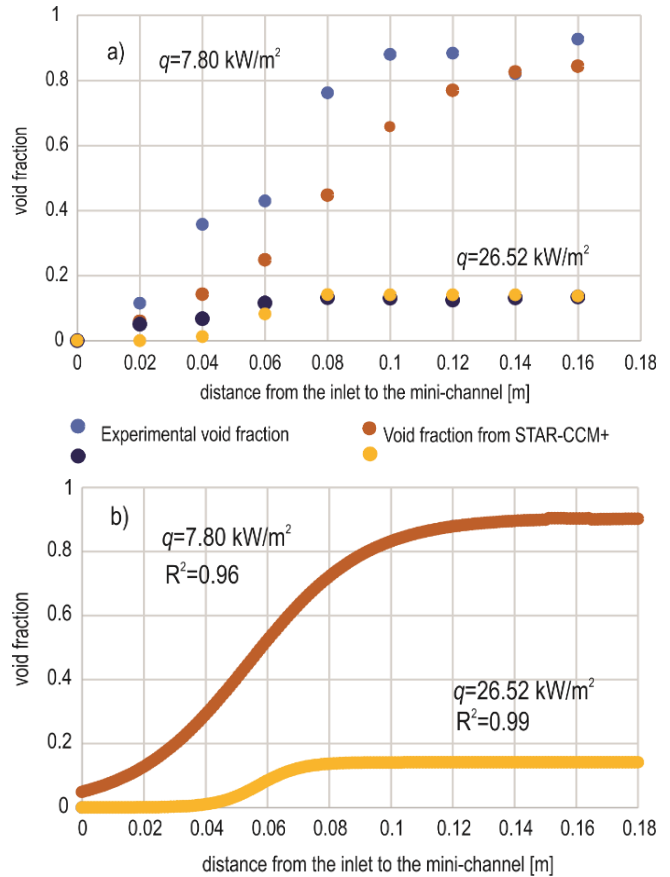


Fig. 5. (a) Experimental void fraction obtained from calculations using the STAR-CCM+ program, (b) Void fraction approximation with the logistic curve; experimental data: heat flux $q = 7.80 \text{ kW/m}^2$ and $v_{ave} = 0.011 \text{ m/s}$, heat flux $q = 26.52 \text{ kW/m}^2$ and $v_{ave} = 0.023 \text{ m/s}$

The maximum absolute differences (MAD) are calculated using the following formula:

$$MAD = \max|f - g| \quad (24)$$

where f, g are functions.

The MAD between the experimental void fraction and the void fraction calculated using the STAR-CCM+ program ranged from 0.12 to 0.31, and the largest differences occurred for the smallest heat fluxes ($q = 7.80 \text{ kW/m}^2$) and in the middle part of the mini-channel. The logistic curve approximates the void fraction very well, where the smallest coefficient of determination R^2 was 0.95. There is an increase in the void fraction with the increase in the distance from the inlet to the mini-channel, with slightly higher values for the void fraction approximated by the logistic curve than that obtained from the CFD program. The MAD between the values of both functions (i.e. the logistic curve and the void frac-

tion obtained by STAR-CCM+) do not exceed 0.34, and the largest differences occur in the middle part of the mini-channel.

Fig. 6 shows the temperature of the copper block measured in three points (marked in Fig. 1b) with the temperature distributions obtained by using the TM and STAR-CCM+.

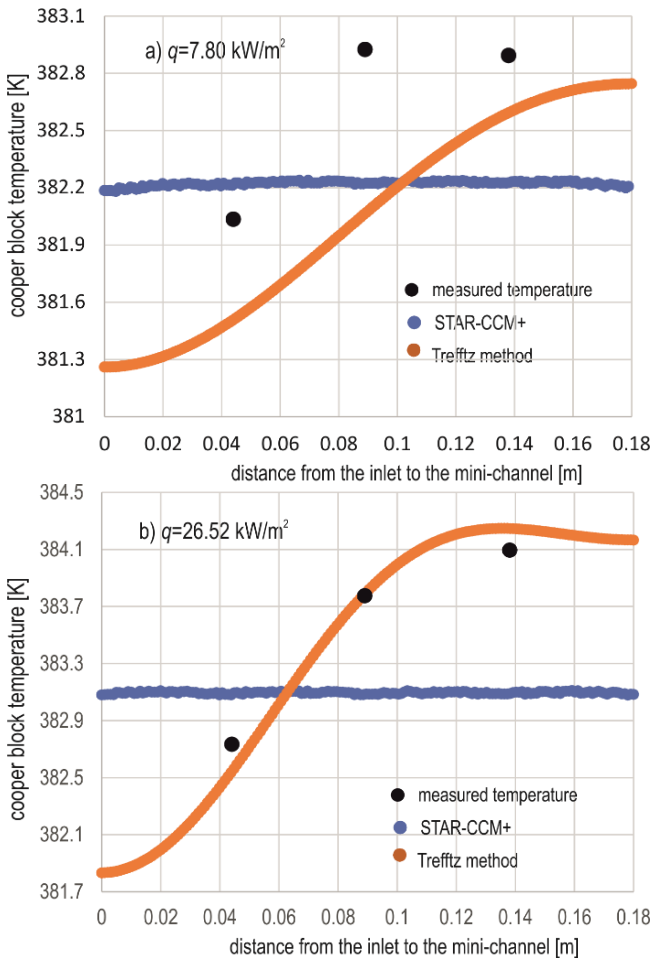


Fig. 6. Temperature of the copper block measured in three points and the temperature obtained by using the TM and STAR-CCM+ program; experimental data: (a) heat flux $q = 7.80 \text{ kW/m}^2$, (b) heat flux $q = 21.90 \text{ kW/m}^2$

To compare the measured and computed temperatures of the copper block, the maximum average relative difference (MARD) calculated from the formula are used:

$$\text{MARD} = \max\left(\frac{\|f-g\|}{\|f\|}, \frac{\|f-g\|}{\|g\|}\right) \quad (25)$$

where $\| \cdot \|$ denoted L^2 norm.

The MARD and MAD for considered results are presented in Tab. 6.

Fig. 7 shows the course of water temperature variability along the flow axis obtained by the TM and numerical simulations performed in STAR-CCM+ for various heat fluxes. The water temperature for both numerical approaches has similar values; the MAD between the results range from 5.33 K to 9.17 K (the largest difference is for heat flux $q = 21.90 \text{ kW/m}^2$). The MARD do not exceed 1%.

Tab. 6. MARD and MAD values.

Compared results	MARD [%]	MAD [K]
The cooper block temperature measurements and results obtained by STAR-CCM+	0.14–0.26	0.56–1.01
The cooper block temperature measurements and results obtained by the TM	0.03–0.22	0.1–0.86
Temperature of the cooper block obtained by the TM and STAR-CCM+	0.09–0.33	0.89–1.25

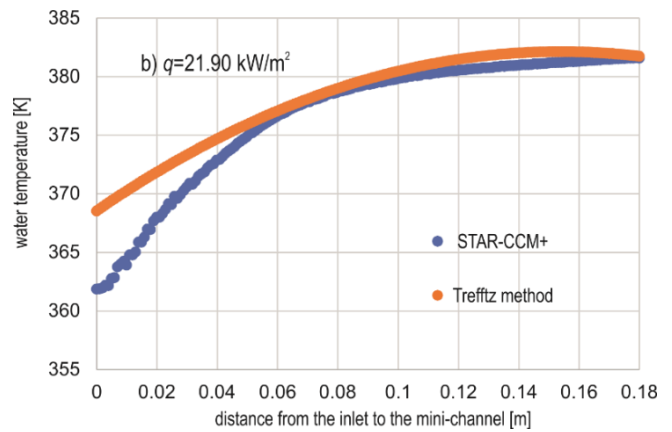


Fig. 7. Water temperature distribution along the flow axis obtained by the TM and STAR-CCM+ program; experimental data: (a) heat flux $q = 7.80 \text{ kW/m}^2$ and $v_{ave} = 0.011 \text{ m/s}$, (b) heat flux $q = 21.90 \text{ kW/m}^2$ and $v_{ave} = 0.011 \text{ m/s}$. TM, Trefftz method

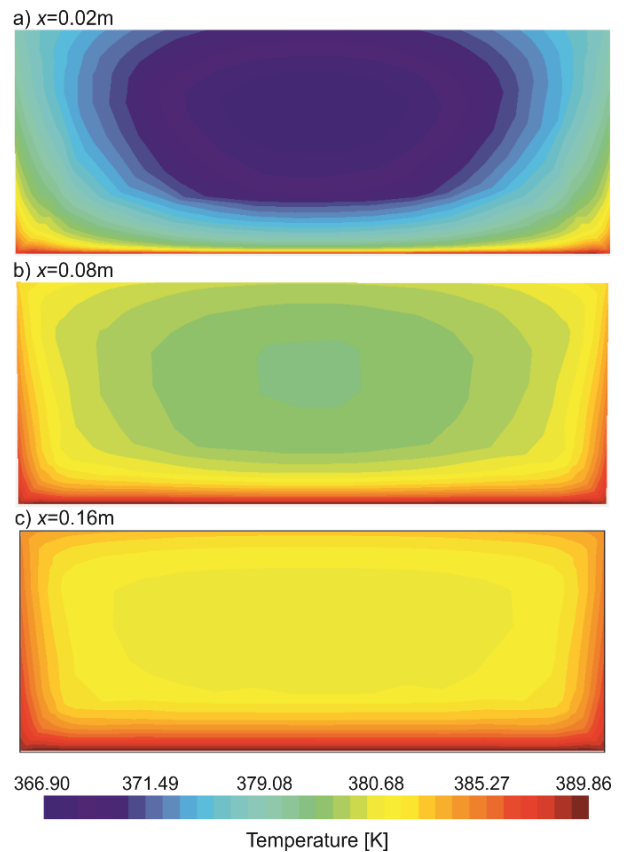


Fig. 8. Temperature distribution of fluid in three cross-sections perpendicular to the flow direction: (a) $x = 0.02 \text{ m}$, (b) $x = 0.08 \text{ m}$, (c) $x = 0.16 \text{ m}$ and heat flux $q = 21.90 \text{ kW/m}^2$

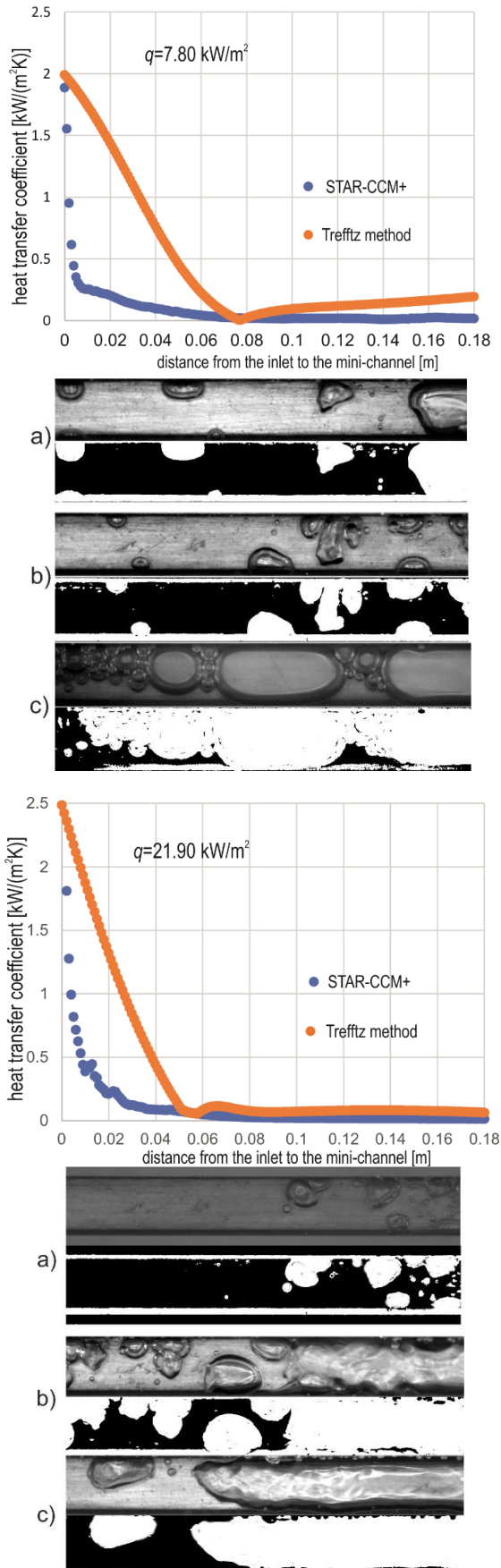


Fig. 9. Heat transfer coefficient obtained by the TM and STAR-CCM+ program. Below the graph, there are photos of two-phase structures and phase contours for the distance from the beginning of the channel: (a) 0.04 m, (b) 0.1 m, (c) 0.16 m. TM, Trefftz method

Fig. 8 shows temperature distributions in selected cross-sections ($x = 0.02$ m, $x = 0.08$ m, $x = 0.16$ m) of the fluid flow in the mini-channel. Temperature fields are determined based on a model of a homogeneous two-phase mixture. The actual course of boiling deviates from this strong assumption, and clustered phase structures of liquid and vapour are observed. However, from the point of view of the averaged parameters, it is assumed that both approaches are equivalent. The model of a homogeneous two-phase mixture allows a good reflection of the temperature field in the cross-section of the fluid flow, which is well correlated with the probability of the appearance of vapour bubbles in the real flow.

The dependence of the heat transfer coefficient as a function of distance from the inlet to the mini-channel is shown in Fig. 9, with a visible decrease in the growing distance. It is the effect of the increasing void fraction in the mini-channel (Fig. 5). The heat transfer coefficient calculated using CFD software “quickly” decreases compared to the coefficient calculated using the TM. The greatest differences between the values of heat transfer coefficients can be noticed in the initial section of the mini-channel, with the average difference between them reaching $1.6 \text{ kW}/(\text{m}^2 \text{ K})$. The largest differences between the results are achieved for the lowest heat flux.

The effectiveness of the adopted computational grid was examined and assessed using the grid convergence method (GCI). Calculations were carried out for three different grids, with the grid refinement factor >1.3 . The values of the numerical uncertainty GCI_{21} in the fine-grid solution range from 0.09% to 0.40% (see Tab.3). As can be seen from Tab. 4, expanded uncertainty (at a confidence level of 95%) of the discretisation error for the three selected grids in presented experiments does not exceed 0.6%.

5. CONCLUSIONS

The article describes the study of saturated boiling during the flow of distilled water through an asymmetrically heated mini-channel.

The results of experiments were the basis for numerical calculations. To solve the heat transfer problem, two numerical approaches were used: one approach was based on the Trefftz functions and the other based on the Simcenter STAR-CCM+ program. Inverse heat transfer problem was solved using the TM, while a direct heat transfer problem was solved using the Simcenter STAR-CCM+ program.

The following conclusions can be drawn from the experiments and the analysis of the results obtained using the TM and the simulation in CFD software:

- The results of CFD simulations are consistent with the results obtained by using the TM and the results of the experiment. The obtained MAD are at a low level, which allows validation of the CFD model and the calculations by the TM.
- In selected experiments presented in this article, the value of the heat transfer coefficient determined by using the TM is higher than the heat transfer coefficient obtained from CFD simulations. The most significant differences were observed near the mini-channel inlet, and the average difference did not exceed $1.6 \text{ kW}/(\text{m}^2 \text{ K})$.
- Regardless of the method used for determining the heat transfer coefficient, the coefficient decreased with the increase in the distance from the inlet to the mini-channel, which was accompanied by an increase in the void fraction local value.

- Expanded uncertainty (at a confidence level of 95%) of the discretisation error for three selected grids in the presented experiments does not exceed 0.6%

The advantage of CFD software lies in the ability to obtain a solution in domains with complex shapes and comprehensive analysis of results with their visualisation. It is worth noting that STAR CCM+ software requires discretisation of the studied domain, which leads to some simplifications and inaccuracies. The TM can bypass this problem by solving differential equations in the whole domain without meshing, which helps avoid discretisation errors. Additionally, the TM enables flexible incorporation of boundary conditions to the error functional, thus leading to a better representation of real conditions.

The planned experimental studies are aimed at time-dependent and non-adiabatic flows in mini-channels and modification of the two-dimensional model and the TM. It is also planned to use CFD software in research, which will allow reducing the experimental part in favour of numerical simulations. However, it should be kept in mind that the results of numerical simulations should always be verified by the results of the experiment.

REFERENCES

1. Kandlikar SG. History, advances, and challenges in liquid flow and flow boiling heat transfer in microchannels: a critical review. *J Heat Transf ASME*. 2012;134(3):Article Number: 034001.
2. Kharangate C, O'Neill LE, Mudawar I. Effects of two-phase inlet quality, mass velocity, flow orientation, and heating perimeter on flow boiling in a rectangular channel: Part 1 – Two-phase flow and heat transfer results. *Int J Heat Mass Transf*. 2016;103:1261–1279.
3. Placzkowski K, Grabowski M, Poniewski ME. Novel twofold use of photographic technique for simultaneous flow boiling image recording and void fraction computation in a minichannel experiment. *Energies*. 2021;14:4478.
4. Amalfi RL, Vakili-Farahani F, Thome JR. Flow boiling and frictional pressure gradients in plate heat exchangers. Part 2: Comparison of literature methods to database and new prediction methods. *Int J Refrig*. 2016;61:185–203.
5. Cheng L, Xia G. Fundamental issues, mechanisms and models of flow boiling heat transfer in microscale channels. *Int J Heat Mass Transf*. 2017;108:97–127.
6. Layssac T, Lips S, Revellin R. Effect of inclination on heat transfer coefficient during flow boiling in a mini-channel. *Int J Heat Mass Transf*. 2019;132:508–18.
7. Grabowski M, Hozejowska S, Maciejewska B, Placzkowski K, Poniewski ME. Application of the 2-D Trefftz Method for Identification of Flow Boiling Heat Transfer Coefficient in a Rectangular MiniChannel. *Energies*. 2020;13:3973. <https://doi.org/10.3390/en13153973>.
8. Tentner A, Merzari E, Vegendla P. Computational fluid dynamics modeling of two-phase boiling flow and critical heat flux. In: *2nd Int Conf on Nuclear Engineering ICONE22*. Prague; 2014. p. 1–9.
9. Guo Z, Fletcher DF, Haynes BS. Numerical simulation of annular flow hydrodynamics in microchannels. *Comput Fluids*. 2016;133:90–102.
10. Colombo M, Fairweather M. Accuracy of Eulerian–Eulerian, two-fluid CFD boiling models of subcooled boiling flows. *Int J Heat Mass Transf*. 2016;103:28–44.
11. Li Z, Pan J, Peng H, Chen D, Lu W, Wu H. Numerical study on subcooled flow boiling in narrow rectangular channel based on OpenFOAM. *Prog Nucl Energy*. 2022;154(104451). <https://doi.org/10.1016/j.pnucene.2022.104451>.
12. Thome JR, Dupont V, Jacobi AM. Heat transfer model for evaporation in microchannels . Part I : presentation of the model. *Int J Heat Mass Transf*. 2004;47:3375–85.
13. Dupont V, Thome JR, Jacobi AM. Heat transfer model for evaporation in microchannels . Part II : comparison with the database. *Int J Heat Mass Transf*. 2004;47:3387–401.
14. Anjos G, Mangiavacchi N, Borhani N, Thome JR. 3D ALE finite-element method for two-phase flows with phase change. *Heat Transf Eng*. 2014;35(5):537–547.
15. Çebi A, Celen A, Donmez A, Karakoyun Y, Celen P, Celtek MS, Taner T, Wongwises S. No Title. *J Therm Eng*. 2018;4(3):2037–74.
16. Elahi M, Soudagar M, Kalam M., Sajid MU, Afzal A, Banapurmath RN, Akram N, Mane SD, Saleel CA. Thermal analyses of minichannels and use of mathematical and numerical models. *Numer Heat Transf Part A Appl*. 2020;77(5):1–41.
17. Guo Z, Fletcher DF, Haynes BS. A review of computational modelling of flow boiling in microchannels. *J Comput Multiph Flows*. 2014;6(2):79–110.
18. Gupta R, Fletcher DF, Haynes BS. Taylor flow in microchannels: a review of experimental and computational work. *J Comput Multiph Flows*. 2010;2(1):1–31.
19. Qian H, Hrnjak P. Design and calibration of capacitive sensors for measuring void fraction in vertical headers of microchannel heat exchangers. *Int J Refrig*. 2021;129:Pages 224–236.
20. Libert N, Morales REM, Silva MJ. Capacitive measuring system for two-phase flow monitoring. Part 1: Hardware design and evaluation. *Flow Meas Instrum*. 2016;47:90–99.
21. Libert N, Morales REM, Silva MJ. Capacitive measuring system for two-phase flow monitoring. Part 2: Simulation-based calibration. *Flow Meas Instrum*. 2016;50:102–111.
22. Cavaro M. A void fraction characterization by low frequency acoustic velocity measurements in microbubble clouds. *Phys Procedia*. 2015;70:496 – 500.
23. Gardenghi AR, Filho ES, Chagas DG, Scagnolatto G, Oliveira RM, Tibirica CB. Overview of void fraction measurement techniques, databases and correlations for two-phase flow in small diameter channels. *Fluids*. 2020;5(216):1–26.
24. Trefftz E. Ein Gegenstück zum Ritzschen Verfahren, Zurich, Switzerland, Sep. 12-17. In: *Proc Int Kongress für Technische Mechanik*. Zürich; 1926. p. 131–7.
25. Ciałkowski M, Olejnik A, Joachimiak M, Grysa K, Frąckowiak A. Cauchy type nonlinear inverse problem in a two-layer area. *Int J Numer Methods Heat Fluid Flow*. 2022;32(1):313–331. <https://doi.org/10.1108/HFF-09-2020-0584>.
26. Maciąg A, Pawińska A. The solution of nonlinear direct and inverse problems for beam by means of the Trefftz functions. *Eur J Mech - A/Solids*. 2022;92:104476. <https://doi.org/10.1016/j.euromechsol.2022.104476>.
27. Grysa K, Maciejewska B. Trefftz functions for non-stationary problems. *J Theor Appl Mech*. 2013;51(2):251–64.
28. Hozejowski L, Hozejowska S. Trefftz method in an inverse problem of two-phase flow boiling in a minichannel. *Eng Anal Bound Elem*. 2019;98:27–34. <https://doi.org/10.1016/J.ENGANABOUND.2018.10.001>.
29. Liu CS. A modified collocation Trefftz method for the inverse Cauchy problem of Laplace equation. *Eng Anal Bound Elem*. 2008;32(9):778–785. <https://doi.org/10.1016/j.enganabound.2008.08.001>.
30. Qin QH. *The Trefftz Finite and Boundary Element Method*. Southampton: WIT Press; 2000.
31. Piasecka M, Piasecki A, Dadas N. Experimental Study and CFD Modeling of Fluid Flow and Heat Transfer Characteristics in a Mini-channel Heat Sink Using Simcenter STAR-CCM+ Software. *Energies*. 2022;15(536):1–20. <https://doi.org/10.3390/en15020536>.
32. Belgacem F Ben, Fekih H El. On Cauchy's problem: I. A variational Steklov–Poincaré theory. *Inverse Probl*. 2005;21(6):1915–1936. <https://doi.org/10.1088/0266-5611/21/6>.
33. Hirt C., Nichols B. Volume of fluid (VOF) method for the dynamics of free boundaries. *J Comput Phys*. 1981;39(1):201–225. [https://doi.org/10.1016/0021-9991\(81\)901.0](https://doi.org/10.1016/0021-9991(81)901.0).
34. Eymard R, Gallouët T, Herbin R. Finite volume methods. *Handb Numer Anal*. 2000;7:713–1018. [https://doi.org/10.1016/S1570-8659\(00\)0](https://doi.org/10.1016/S1570-8659(00)0).

35. Roache PJ. Perspective: A Method for Uniform Reporting of Grid Refinement Studies. *J Fluids Eng ASME*. 1994;116(3):405–13.
36. Celik IB, Ghia U, Roache PJ, Freitas CJ. Procedure for Estimation and Reporting of Uncertainty Due to Discretization in CFD Applications. *J Fluids Eng ASME*. 2008;130(7):1–4.
37. Richardson LF. The Approximate Arithmetical Solution by Finite Differences of Physical Problems Involving Differential Equations, With an Application to the Stresses in a Masonary Dam. *Philos Trans R Soc A*. 1911;210:307–357.
38. Richardson LF. The Deferred Approach to the Limit. *Philos Trans R Soc A*. 1927;226:299–361.
39. Roache PJ. Quantification of Uncertainty in Computational Fluid Dynamics. *Annu Rev Fluid Mech*. 1997;29:123–60.
40. Johnson RW, Schultz RR, Roache PJ, Celik IB, Pointer WD, Hassan YA. Processes and Procedures for Application of CFD to Nuclear Reactor Safety Analysis. U.S. Department of Energy Office of Scientific and Technical Information. 2006.

Acknowledgements: The research reported herein was funded partially by the National Science Centre, Poland, grant No. UMO-2018/31/B/ST8/01199.

Beata Maciejewska:  <https://orcid.org/0000-0002-4692-7560>

Sylwia Hożejowska:  <https://orcid.org/0000-0003-2558-5132>

Mirosław Grabowski:  <https://orcid.org/0000-0001-5057-4158>

Mieczysław E. Poniewski:  <https://orcid.org/0000-0003-2458-6299>



This work is licensed under the Creative Commons BY-NC-ND 4.0 license.